

pubs.acs.org/JPCL Letter

# Enhanced CINO<sub>2</sub> Formation at the Interface of Sea-Salt Aerosol

Seokjin Moon and David T. Limmer\*



Cite This: J. Phys. Chem. Lett. 2024, 15, 9466-9473



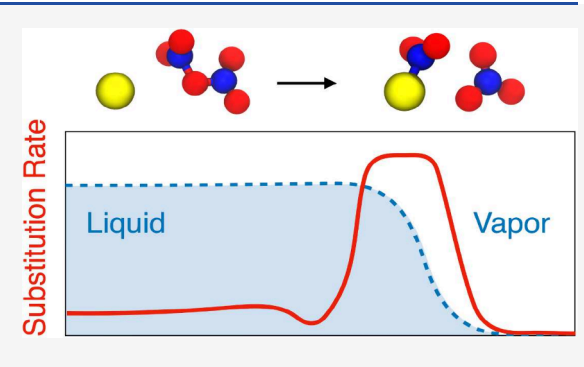
**ACCESS** 

Metrics & More

Article Recommendations

SI Supporting Information

**ABSTRACT:** The reactive uptake of  $N_2O_5$  on sea-spray aerosol plays a key role in regulating the  $NO_x$  concentration in the troposphere. Despite numerous field and laboratory studies, a microscopic understanding of its heterogeneous reactivity remains unclear. Here, we use molecular simulation and theory to elucidate the chlorination of  $N_2O_5$  to form  $ClNO_2$ , the primary reactive channel within sea-spray aerosol. We find that the formation of  $ClNO_2$  is markedly enhanced at the air—water interface due to the stabilization of the charge-delocalized transition state, as evident from the formulation of bimolecular rate theory in heterogeneous environments. We explore the consequences of the enhanced interfacial reactivity in the uptake of  $N_2O_5$  using numerical solutions of molecular reaction-diffusion equations as well as their analytical approximations. Our



results suggest that the current interpretation of aerosol branching ratios needs to be revisited.

When trace gas molecules collide with an aerosol particle, a mass accommodation process transports them into the bulk of the aerosol, where some are lost irreversibly to subsequent chemical reactions. The efficiency of this heterogeneous reactive uptake plays a crucial role in global-scale environmental processes.  $^{1,2}$  The uptake efficiency depends on elementary steps—including adsorption, desorption, diffusion and reaction—whose relative importance in heterogeneous environments is challenging to anticipate. Surface-specific spectroscopy  $^{4,5}$  and molecular simulations  $^{6,7}$  have revealed that the physical and chemical properties of a molecularly thin region around the air—water interface are distinct from either of the surrounding bulk phases, complicating studies of heterogeneous uptake. We have developed a molecular model of this complex interface to understand the uptake of  $\rm N_2O_5$  to form CINO2 on the surface of a sea-salt aerosol.

The uptake of  $N_2O_5$  by aerosol has been investigated to understand the fate of tropospheric  $NO_x$  at night. Tropospheric  $NO_x$  radicals are the primary source of hydroxyl radical and catalyze ozone production. A global chemistry transport model estimated 41% of  $NO_x$  is consumed through the heterogeneous reactive uptake of  $N_2O_5$ . The key parameter for the global model is the reactive uptake coefficient,  $\gamma$ , a ratio of the irreversibly lost reactive flux to the kinetic surface collision flux. Interpretation of the measured variation of  $\gamma$  in terms of aerosol composition and meteorological conditions demands a microscopic perspective, which ultimately would enable the prediction and parametrization of  $\gamma$ . For sea-spray aerosols, arguably the two most important reactions determining the uptake of  $N_2O_5$  are

$$N_2O_{5(g)} + H_2O_{(1)} \xrightarrow{k_H} 2HNO_{3(aq)}$$
 (R1)

$$N_2O_{5(g)} + Cl_{(aq)}^- \xrightarrow{k_C} ClNO_{2(aq)} + NO_{3(aq)}^-$$
 (R2)

hydrolysis to nitric acid (R1) and chlorination to  $ClNO_2$  (R2). Atomistic simulations based on machine-learning force fields have provided thermodynamic and mechanistic detail into the hydrolysis reaction (R1).<sup>6,7</sup> However, a complementary microscopic understanding of the chlorination reaction (R2) is lacking.<sup>15</sup>

Early studies of R2 with cryogenic vibrational spectroscopy observed a stable ion-dipole complex,  $[ClN_2O_5]^-$ , illustrating the plausibility of an  $S_N^2$ -type reaction mechanism. Subsequent first-principles calculations have found low-lying reaction pathways in water clusters consistent with this perspective. While some phenomenological evidence suggests that both R1 and R2 proceed by a two-step pathway including predissociation of  $N_2O_5$  into  $NO_3^-$  and  $NO_2^+$  throughout this manuscript we assume that both reactions are concerted. For an  $S_N^2$ -type charge transfer reaction with  $Cl^-$ , solvent molecules around the solute need to be collectively rearranged to accommodate the distinct charge distribution of the product. As a consequence, the role of the heterogeneous environment cannot be ignored for this reaction. Molecular

Received: August 2, 2024
Revised: August 30, 2024
Accepted: September 4, 2024
Published: September 10, 2024





dynamics simulations with a reactive model we developed based on the empirical valence bond approach suggest that the chlorination rate is significantly enhanced in the vicinity of the air—water interface. The important role of the solvent degrees of freedom emerged naturally from analysis of the commitment probability. On

Understanding how an enhanced reaction rate at the airwater interface contributes to  $\gamma$  requires a mass transport equation. Continuum reaction-diffusion equations are widely used,<sup>21</sup> which describe diffusive dynamics of various chemical species with their reactivity. However, most are phenomenological in that bulk transport properties are used for their parametrization.<sup>22</sup> We formulate the molecularly detailed reaction-diffusion equation for N2O5 with two reaction channels (R1 and R2). Numerical solutions with various bulk Cl<sup>-</sup> concentrations are compared with experimental measurements and challenge the previous analytical framework based on bulk-dominant and homogeneous reactivity. Moreover, analytic expressions from the resistor model with theoretically informed parametrization are compared with the numerical results, showing good agreement. The novel kinetic framework, together with the molecular simulations, paves the way to systematically incorporate heterogeneous reactivity to the analysis of the reactive uptake process.

The air-water interface is a molecularly thin environment, where the solvent behaves in a manner distinct from its bulk aqueous phase. The reduced amount of solvent at the interface results in an altered thermodynamic cost to rearrange the hydrogen-bonding structure, which influences the affinities of reactants to the interface as well as the rate of reactions driven by electrostatic fluctuations near it. <sup>23–26</sup> To provide a balanced description of both reactivity and the long-ranged electrostatic environment of an explicit air-water interface, we developed a novel empirical valence bond model. We built our model by constructing two low-lying diabatic states, encoding the reactant and product states of R2. The diabatic Hamiltonian for each state was reparameterized from the generalized Amber force field.<sup>27</sup> The point charges on each atom were optimized to reproduce the interfacial affinities of each species estimated from higher levels of theory. 7,28 The two diabatic states were coupled through a diabatic coupling Hamiltonian modeled as a linear combination of multiple Gaussians<sup>29</sup> and fitted to reproduce the gas-phase potential energy surface computed with the range-separated hybrid density functional, ωB97X-V/DEF2-TZVPD<sup>30</sup> (Supporting Information Figure S1). The water was modeled using the flexible variant of SPC/Fw.<sup>31</sup> Further details are provided in the Supporting Information Section 1. With the reactive model, we simulated the air—water interface using a slab geometry consisting of 512 water molecules, a single N<sub>2</sub>O<sub>5</sub>, and one excess of Cl<sup>-</sup>. A schematic picture of the system is shown in Figure 1a.

The reversible work for moving a molecule perpendicular to the interface measures its interfacial propensity. We evaluate the reversible work, or the free energy profile, for each chemical species in R2 as a function of the depth from the interface,  $F_i(z) = -k_{\rm B}T \ln \langle \delta(z-z_c^i) \rangle$ , where  $z_c^i$  is the center of mass of species i relative to the Gibbs dividing surface,  $k_{\rm B}T$  is Boltzmann's constant times temperature, and the brackets surrounding the Dirac delta function denote a canonical ensemble average at fixed temperature 298 K. Umbrella sampling with harmonic biasing potentials was applied to evaluate these averages,  $^{32}$  and histograms of z from such

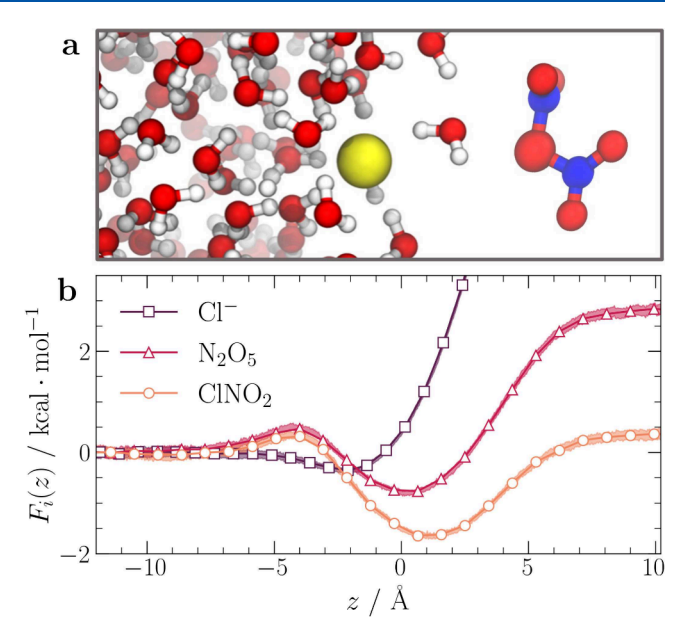


**Figure 1.** (a) Schematic picture of the air—water interface system with chemicals in (R2). (b) Reversible work as a function of the center-of-mass z location for each species  $i = \operatorname{Cl}^-$ ,  $\operatorname{N}_2\operatorname{O}_5$ , and  $\operatorname{ClNO}_2$ . The Gibbs dividing surface is located at z = 0 Å. Positive and negative z correspond to the bulk gas and solution sides, respectively. Errors represent 1 standard error.

simulations were reweighted using the weighted histogram analysis method<sup>33</sup> to compute an unbiased estimate of  $F_i(z)$ .

The resultant free energy profiles for Cl<sup>-</sup>, N<sub>2</sub>O<sub>5</sub>, and ClNO<sub>2</sub> are shown in Figure 1b. The two neutral molecules, N<sub>2</sub>O<sub>5</sub> and ClNO<sub>2</sub>, are locally stabilized around the air-water interface, and both face free energy barriers to move from the interface into either the bulk vapor or bulk solution phase. This is due to the weak interactions with surrounding water molecules, resulting in an enriched concentration of both species at the interface relative to the bulk. By contrast, strong ion-water interactions prevent Cl<sup>-</sup> from penetrating into the vapor,<sup>34</sup> which is evident from the stiff rise of the free energy starting at z = 0 Å. A slight stabilization of Cl<sup>-</sup> around the interface is consistent with some surface-specific spectroscopy measurements.4 While the adsorption free energy of chloride is consistent with current sophisticated polarizable models (Supporting Information Section 1), we acknowledge that persistent uncertainty exists with its experimental value.

The free energy difference between the gas and aqueous phases is related to a well-known descriptor of solubility known as Henry's law constant. Direct measurements of the Henry's law constant for  $N_2O_5$  are limited due to its facile hydrolysis. Indirect measurements report a value of  $H=4.9~\mathrm{M/atm},^{35}$  which is close to our estimate of  $H=4.8~\mathrm{M/atm}$ . For  $\mathrm{ClNO}_2$ , lab measurements report  $H=0.024~\mathrm{M/atm}^{36}$  and we estimate  $H=0.040~\mathrm{M/atm}$ . A lower value of H indicates more volatile nature of  $\mathrm{ClNO}_2$  compared to  $\mathrm{N_2O_5}$ . Considered in conjunction with the expected exothermic forward reaction with  $\mathrm{Cl}^{-17,18}$  the role of the backward reaction of  $\mathrm{R2}$  is considered to be negligible in the uptake process.

The substitution reaction in R2 is expected to be concerted. A canonical order parameter for describing it would be  $\xi = r_1 - r_2$ , which is defined as a bond-length difference between bond-breaking and bond-forming pairs. In this case, the leaving group is the nitrate anion, and so we take  $r_2$  to be the distance

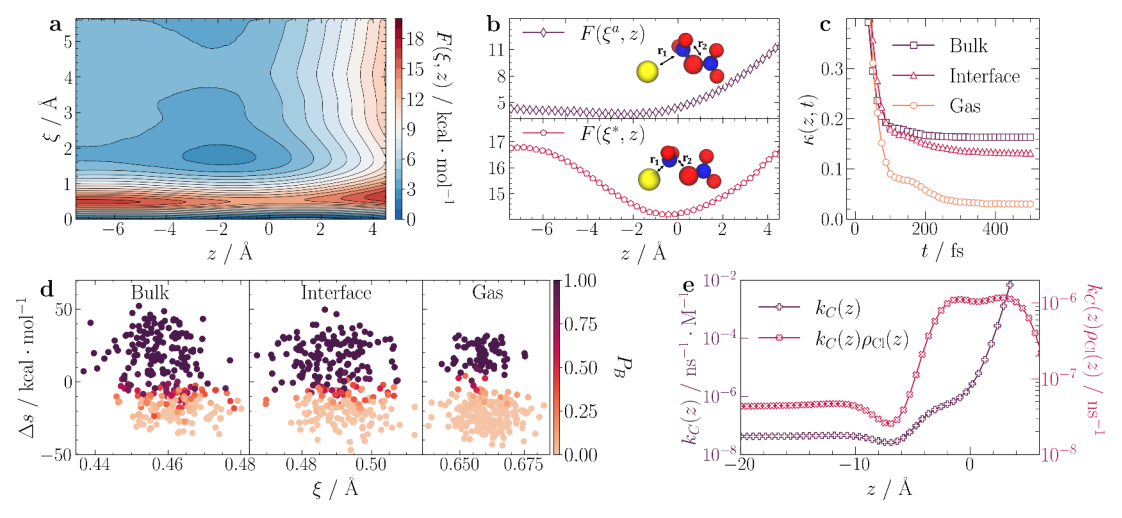


Figure 2. (a) Free energy surface as a function of the  $S_N 2$  order parameter  $\xi$  and depth z of  $Cl^-$ . (b) Conditional free energy profile along z for the reactant ( $\xi^a = 5.62$  Å) and transition state ( $\xi^* = 0.52$  Å), with schematic pictures of states. (c) Transmission coefficients measured at three distinct z constraints. (d) Commitment probability as a function of  $\xi$  and solvents' degrees of freedom  $\Delta s$  at three z values. (e) Heterogeneous bimolecular rate (left y-axis) and pseudo first-order loss rate of  $N_2O_5$  (right y-axis) corresponding to 1 M of bulk  $Cl^-$  density. For (c) and (d), the z values correspond to Bulk (z = -12.3 Å), Interface (z = 0 Å) and Gas (z = 5 Å).

between the center oxygen on  $N_2O_5$  and the nitrogen forming ClNO<sub>2</sub>. The nucleophile is Cl<sup>-</sup>, and so we take  $r_1$  to be the distance between it and the same nitrogen. While  $\xi$  is sufficient to differentiate the reactant and product states in a bulk solution, it does not discriminate between the reactions occurring at or away from the air—water interface. In order to clarify the thermodynamics of the reaction and how it depends on the proximity to the interface, we consider the free energy surface defined by both  $\xi$  and the z position of Cl<sup>-</sup>. The resultant free energy,  $F(\xi, z) = -k_B T \ln \langle \delta(z - z_c^{\text{Cl}}) \delta(\xi - r_1 + r_2) \rangle$  is computed in an analogous manner to its marginal  $F_{\text{Cl}}(z)$  using umbrella sampling and histogram reweighting.

Figure 2a depicts  $F(\xi, z)$  in the vicinity of the Gibbs dividing surface. Three states are evident along constant z slices: a reactant state where Cl<sup>-</sup> is distant from N<sub>2</sub>O<sub>5</sub> with  $\xi \geq 5.62$  Å, an ion-dipole complex for  $\xi \sim 2$  Å, and a transition state whose free energies are local maxima occurring near  $\xi \sim 0.5$  Å. The free energetics of the reaction share common features across *z*; the ion-dipole complex is metastable, and the reaction is strongly exothermic. The ion-dipole complex is most metastable at the interface due to the interplay of incomplete dielectric screening and partial solvation. The stabilization of the reactant and the barrier height also show variations near the interface. This is illustrated in Figure 2b, where constant  $\xi$ slices of the free energy surface are shown;  $F(\xi^a, z)$  for the reactant state and  $F(\bar{\xi}^*, z)$  for the transition state. The z dependence of the reactant free energy mirrors the stability of Cl<sup>-</sup>, which is thermodynamically unfavorable to desolvate. The z dependence of free energy at the transition state is nonmonotonic, exhibiting a minimum at the Gibbs dividing surface. The lowering of the barrier height from the bulk solution to the interface is significant, nearly 3 kcal·mol<sup>-1</sup>.

The transition state of the  $\rm S_N 2$  reaction described by our model has a delocalized charge distribution, with half of the negative charge transferred to the nitrate ion. Our model potential energy surface in the gas phase exhibits a sub-kcal-mol<sup>-1</sup> barrier due to the facile ability of  $\rm N_2O_5$  to dissociate. Hence, the gas-phase reaction is expected to proceed at the diffusion limit, like most ion-dipole chemistry. In the bulk solution phase, the thermodynamic penalty for distributing the

charge across the Cl and NO<sub>3</sub> species results in a significant free energy barrier. The destabilization results from the relatively unfavorable solvation free energy of the delocalized charge distribution and is the origin of the slow reaction kinetics in polar solvents that have been observed experimentally<sup>37</sup> and theoretically.<sup>38</sup> The existence of the minimum in the barrier height at the interface reflects the competing factors affecting the solvation of charged species at the airwater interface.<sup>39,40</sup> The charge-delocalized transition state behaves similarly to large anions that have shown preferential adsorption due to a combination of favorable excluded volume factors arising because of facile density fluctuations and unfavorable electrostatic contributions such as repulsive image charge interactions.<sup>41</sup>

Connecting the free energetics of the reaction to its rate requires rate theory. To describe the process in R2, we need to generalize the standard bimolecular rate theory for a heterogeneous environment. Detailed discussion on the derivation of such a generalization can be found in Supporting Information Section 2, but it follows from manipulating the usual side—side correlation function and imposing a conditioning on the reaction occurring at a fixed z position. Within a reactive flux formulation, the bimolecular rate can be written as a product of a position dependent transmission coefficient  $\kappa(z)$  and a transition state theory (TST) approximation to the rate,  $k_{\rm C}^{\rm TST}(z)$ 

$$k_{\mathrm{C}}^{\mathrm{TST}}(z) = \left[ \sqrt{\frac{k_{\mathrm{B}}T|\mathbf{G}|}{2\pi}} \frac{3}{r_{\mathrm{I}}^{a}} e^{-\Delta F(z)/k_{\mathrm{B}}T} \right] \nu(z) \tag{1}$$

where  $\Delta F(z) = F(\xi^*,z) - F(\xi^a,z)$  is the barrier height at fixed z and |G| is the inverse effective mass of  $\xi$ . The factor  $\nu(z)$  accounts for the local density enhancement of  $N_2O_5$  and is given by

$$\nu(z) = \int_0^{r_1^d} r^2 dr \int d\Omega e^{-[F_N(z+r\cos{(\theta)}) - F_N(z)]/k_B T}$$
 (2)

where  $d\Omega = \sin(\theta)d\theta d\phi$  are polar angles oriented along z, and  $F_{\rm N}(z)$  is the free energy profile of N<sub>2</sub>O<sub>5</sub> shown in Figure 1b. The local N<sub>2</sub>O<sub>5</sub> density is averaged over a size given as  $r_{\rm d}^a$ .

determined by where the free energy obtains an asymptotic scaling,  $F(\xi,z) = F(\xi^a,z) - 2k_BT \ln{(r_1/r_1^a)}$  and  $\xi$  is well approximated by  $r_1$ , i.e.  $\xi^a \approx r_1^a$ . The detailed derivation is provided in Supporting Information Section 2. The expression incorporates two contributions. The part in the square brackets accounts for the barrier crossing frequency if  $N_2O_5$  is constrained in the sphere of radius  $r_1^a$  centered on  $Cl^-$ . This frequency depends on the free energy barrier to the transition state from the reactant state, not from the ion-dipole state. This is because of the unbounded domain of the bimolecular order parameter,  $\xi$ , which results in an overwhelming probability of being in the separated state compared with the bound state. The factor  $\nu(z)$  accounts for the ratio of the mean density of  $N_2O_5$  inside the sphere to the local density at the z location.

The transmission coefficient,  $\kappa(z)$ , provides a correction to the transition state approximation of the rate by accounting for the recrossing events. Using the Bennett–Chandler approach, 45 we measured it using the time-correlation function,  $\kappa(z,t) = 2\langle \nu(0)h[\xi(t)]\rangle_z^*/\langle |\nu|\rangle$ , where  $\nu$  is a velocity of  $\xi$ , and h is an indicator function which has a value of 1 if  $\xi(t)$  is in the product domain or 0 otherwise. The average is taken over the ensemble of trajectories initialized from the transition state with a specific z value. The asymptotic long-time limit of  $\kappa(z,t)$  in Figure 2c is the correction factor  $\kappa(z)$ , which converged to 0.15 in a bulk aqueous environment, 0.14 at the interface, and 0.045 Å above the interface. Hence, the dynamic correction to the rate is insensitive to the environment unless the reaction occurs far from the condensed phase.

The small values of computed  $\kappa(z)$  suggest that  $\xi$  does not fully describe the relevant reaction coordinate of the transition. To uncover the mechanism, we performed a committor analysis by introducing another order parameter  $\Delta s$ , the solvent's contribution to the reorganization energy. In detail,  $\Delta s$  is the result of subtracting the solvent-solute interaction energy of the product diabatic state from that of the reactant diabatic state.<sup>38</sup> The commitment probability,  $P_B(\xi, \Delta s)$ , measures the relative number of trajectories started from fixed  $\xi$  and  $\Delta s$ , reaching the product state before the reactant state.<sup>20</sup> As such,  $P_B$  quantifies the order parameters' performance, since it is 0.5 if the fixed initial point is a member of the transition state ensemble. As shown in Figure 2d, the isocommitment points are aligned near zero of  $\Delta s$ , indicating the important role of solvent's degrees of freedom. Fluctuations of  $\Delta s$  at a constrained value of  $\xi$  result in the small values of  $\kappa$  computed, and its insensitivity with z demonstrates that the mechanism of a solvent mediated charge transfer is conserved near and from the interface.

The bimolecular rate is given by  $k_{\rm C}(z) = \kappa(z) k_{\rm C}^{\rm TST}(z)$  and is shown in Figure 2e. We observe a markedly enhanced reaction rate at the interface, increasing below the Gibbs dividing surface and steeply rising above it. The rate depends exponentially on the free energy difference between two states in Figure 2b. Thus, the rate enhancement below the interface is mainly attributed to the stability of the transition state, while its steep rise above it is due to the destabilization of Cl<sup>-</sup>. This becomes more apparent when the equilibrium density profile of Cl<sup>-</sup> is multiplied by the bimolecular rate. The density profile can be computed from a bulk density  $\bar{\rho}_{\rm Cl}$  times the marginal free energy for Cl<sup>-</sup>,  $\rho_{\rm Cl}(z) = \bar{\rho}_{\rm Cl} \exp[-F_{\rm Cl}(z)/k_{\rm B}T]$ . The pseudo first-order rate,  $k_{\rm C}(z)\rho_{\rm Cl}(z)$ , with  $\bar{\rho}_{\rm Cl} = 1$  M is also shown in Figure 2e, which shows a clear local peak in the rate by 25 times around the interface relative to the bulk solution.

The subsequent decrease in the rate at large z results from the thermodynamic difficulty of getting the transition state into the gas phase. The variation in the rate occurs across molecular scales and is constant a nanometer away from the interface.

The heterogeneous reactive uptake of  $N_2O_5$  involves a series of physical and chemical processes coupled to the diffusive motion. Hence, a coupled partial differential equation for each process is required to be solved to estimate the reactive uptake coefficient. While analytical solutions are only given for some limiting cases, <sup>46</sup> approximate solutions based on the decoupling of the processes are provided as the resistor model. <sup>47</sup> The resistor model has been widely used as a reasonable framework to analyze measured variations of trace gas uptake coefficients. <sup>21</sup> However, given the significant variation in the substitution rate with position relative to the interface we found, a molecularly detailed reaction-diffusion model is necessary.

We employ an overdamped Fokker–Planck equation for the density of  $N_2O_5$ , parametrized from our molecular dynamics simulations.<sup>48</sup> The time-dependent density profile of  $N_2O_5$ ,  $\rho_N(z, t)$ , satisfies

$$\partial_t \rho_{\rm N} = \partial_z D(z) e^{-\beta F_{\rm N}(z)} \partial_z e^{\beta F_{\rm N}(z)} \rho_{\rm N} - k_{\rm T}(z) \rho_{\rm N} \tag{3}$$

where D(z) is the spatially dependent diffusion coefficient and  $k_{\rm T}(z)=k_{\rm H}(z)+k_{\rm C}(z)\rho_{\rm Cl}(z)$  is the spatially dependent total rate for two reaction channels. Solving eq 3 with an absorbing boundary condition placed at z=6.58 Å, we are able to model the evaporation process without introducing underdamped dynamics. We also use a reflecting boundary condition located at z=-200 nm to model a semi-infinite slab of solution. Propagating the equation from a normalized Gaussian-shaped density profile centered on the Gibbs dividing surface describes a distribution of molecules thermalized at the interface after initial collisions with unit sticking probability. Details on the setups are explained in Supporting Information Section 3. The uptake coefficient  $\gamma$  is measured from the solution of eq 3 as a loss of density due to the reaction,

$$\gamma_{\rm T} = \int_0^\infty dt \int dz k_{\rm T}(z) \rho_{\rm N}(z, t) \tag{4}$$

which in this model competes only with re-evaporation.

Using a step function form for D(z) employed previously with a slightly enhanced interfacial diffusivity relative to the bulk solution,7 we first considered the uptake due to just hydrolysis,  $\overline{\rho}_{Cl} = 0$  M. We found  $k_H = 0.4/\mu s$  results in the experimentally reported value of  $\gamma = 0.036$  for a pure water droplet.<sup>14</sup> This rate is much slower than previous theoretical estimates in the literature, 6,7 while close to experimental estimates, 14 reflecting the slower evaporation rate estimated with our model. Given that the rate depends exponentially on the free energy barrier, this change reflects the varying accuracy of the solvation free energetics.<sup>6</sup> Under these conditions the impact of the spatial dependence of  $k_{\rm H}(z)$  was minor, so we have treated it as a constant. The resulting density profiles obtained by solving eq 3 with finite differences using the optimized form of  $k_{\rm H}(z)$  are shown in Figure 3a. The initial Gaussian distribution relaxes over 100 ns and begins to mirror the equilibrium density determined by  $F_N(z)$ , though with reduced amplitude due to evaporation and hydrolysis.

Next, the hydrolysis and chlorination reactions are considered together. In this two reaction channel problem, the branching ratio or the  $CINO_2$  production yield,  $\Phi$ ,

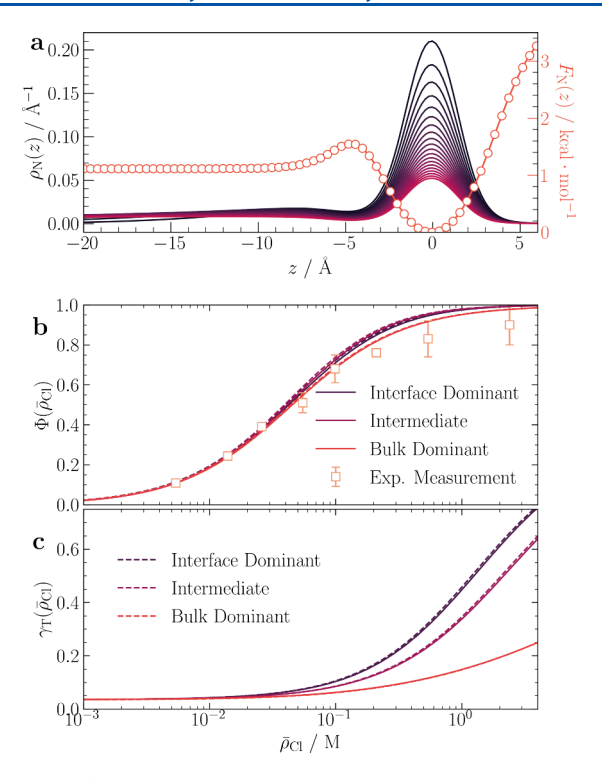


Figure 3. (a) Time-dependent density profiles of  $N_2O_5$  with  $\overline{\rho}_{Cl}=0$ . Curves are separated by 18 ns. The free energy profile of  $N_2O_5$  is shown on the right-axis. (b) ClNO<sub>2</sub> branching ratio measured from eq 5 (solid lines) and the analytic formula (dashed line) as a function of  $\overline{\rho}_{Cl}$ . Flow reactor measurements from Kregel et al. are shown as square markers. (c) Reactive uptake coefficients from eq 4 (solid lines) and the analytic formula (dashed line) as a function of  $\overline{\rho}_{Cl}$ .

becomes a key measurement for analyzing the reactive uptake process. Within our reaction diffusion model, it can be computed from

$$\Phi = \frac{1}{\gamma_{\rm T}} \int_0^\infty dt \int dz \ k_{\rm C}(z) \rho_{\rm CI}(z) \rho_{\rm N}(z, t)$$
 (5)

which is a ratio of the reactive flux into the chlorination channel relative to the total loss due to reactions. Recent experimental measurements have reported  $\Phi$  as a function of bulk Cl<sup>-</sup> concentration, as shown in Figure 3b. 49 We estimated  $\Phi$  using the rate profile  $k_{\rm C}(z)$  from Figure 2c under pseudofirst-order conditions. However, the bare rate predicted from our model is far too slow. Given the gas phase energetics are comparable to high level CCSD(T) calculations in Supporting Information Figure S2, the aqueous reaction barrier is likely overestimated due to overly stabilizing water-solute interactions. If we assume that the shape of rate profile is robust since the enhancement originated from the augmented propensity of the charge-delocalized transition state at the interface, then we can include a multiplicative factor to the rate profile to reproduce the experimental branching ratio of  $\Phi$  = 0.108 with  $\overline{\rho}_{Cl}$  = 0.0054 M and probe the behavior of the system away from that point.

The branching ratio and uptake coefficients using this procedure are summarized in Figure 3b and 3c labeled "Intermediate". We have also considered two additional hypothetical scenarios, an "Interface Dominant" case, whose rate is enhanced by 250 times at the interface, and a "Bulk Dominant" case with zero interfacial rate. Both rate profiles are shifted in the same way as the "Intermediate" case to

reproduce  $\Phi$  at  $\overline{\rho}_{\text{Cl}} = 0.0054$  M (Supporting Information Figure S3). Interestingly the estimated branching ratios show minor differences among the scenarios. However, heterogeneous reactivity at the air—water interface has a pronounced effect on the  $\overline{\rho}_{\text{Cl}}$ -dependent  $\gamma$  (Supporting Information Figure S4). The total uptake coefficient at moderately concentrated solution distinguishes these three clearly, although the simultaneous measurements of the total uptake coefficient with the branching ratio at low concentration have been limited by the gas phase diffusion process experimentally. Finally, in all scenarios, the rise in  $\Phi$  occurs at a lower Cl<sup>-</sup>concentration and then the subsequent rise in  $\gamma$ .

The numerical observations are also compared to simplifying analytic expressions. In the reaction-diffusion formalism, the interfacial reactive loss follows the same first-order kinetics as the evaporation process. Intuited from this, we replaced the role of interfacial reactivity with an increase of evaporation rate and a decrease of Henry's law constant. With the effective kinetics without interfacial reaction, we applied the bulk-dominant resistor model framework. <sup>12,49</sup> As a consequence, we consider the total uptake as  $\gamma = \gamma_{\rm I} + \gamma_{\rm B}(1 - \gamma_{\rm I})$ . The  $\gamma_{\rm I}$  is an ideal interfacial uptake,

$$\gamma_{\rm I} = \frac{k_{\rm I,H} + k_{\rm I,C} \overline{\rho}_{\rm Cl}}{k_{\rm e} + k_{\rm I,H} + k_{\rm I,C} \overline{\rho}_{\rm Cl}} \tag{6}$$

where  $k_{\rm I,H}$  and  $k_{\rm I,C}$  are interfacial rates for hydrolysis and chlorination, respectively, and  $k_{\rm e}$  is the evaporation rate. The bulk uptake

$$\gamma_{\rm B} = \left(\frac{1}{\alpha'} + \frac{\overline{\nu}}{4H'\sqrt{D(k_{\rm B,H} + k_{\rm B,C}\overline{\rho}_{\rm Cl})}}\right)^{-1}$$
(7)

depends on a renormalized mass accommodation coefficient  $\alpha'$  and Henry's law constant H',

$$\alpha' = \frac{k_{s}}{k_{s} + k_{e} + k_{I,H} + k_{I,C}\overline{\rho}_{CI}}, \quad H' = H(1 - \gamma_{I})$$
(8)

where D is the bulk diffusivity,  $\overline{\nu}$  is the molecule's averaged velocity,  $k_{\rm s}$  is the solvation rate, and  $k_{\rm B,H}$  and  $k_{\rm B,C}$  are the bulk rates for hydrolysis and chlorination, respectively. The dashed lines in Figure 3b and 3c are results from the expression, which reproduce the numerical results remarkably well. Notably, this expression reduces to known forms in the limit that the uptake is determined fully by either the bulk or the interfacial processes. This expression is the same as for the resistor model with the interfacial reactivity in the limit that the surface coverage of the ion is negligible.  $^{50,51}$  Detailed derivations are provided in Supporting Information Section 4.

Our molecularly detailed reaction-diffusion equation emphasizes the importance of spatial heterogeneity. Rate profiles whose interfacial contribution varies over 2 orders of magnitude produce the same observable branching ratio, which complicates the traditional interpretation of the branching ratio. For example, weak temperature dependence of the branching ratio was attributed to similar activation barriers for two reactions. However, activation barriers at the interface may differ from the bulk reaction and, so, may need to be considered together. While measurements of  $\Phi$  have provided valuable insights into the competitive nature of two reaction channels, it is clear that the available information is insufficient to conclusively determine the significance of the

interfacial contribution to the overall reactive uptake process. A simultaneous measurement of the total uptake and the branching ratio from experiments on dilute aerosol particles is necessary. Further, for highly concentrated aerosols, reported values of the uptake coefficient are less than 0.04, 12,14 an order of magnitude lower than our prediction even for the bulkdominant reactivity scenario. The discrepancy may be attributed to the ionic correlations omitted from our model. The role of ionic screening effects on reactivity in inhomogeneous environments presents an interesting topic for future research. More broadly, the observation here that a S<sub>N</sub>2 type reaction can be markedly accelerated at a liquidvapor interface due to the stabilization of a charge delocalized transition state suggests a potential origin for recent observations of chemistry in microdroplets and on-water catalysis. 52 The framework employed here using a combination of molecular modeling and theory can be straightforwardly translated into those cases as well.

#### METHODS

**Molecular Dynamics Simulation.** We performed molecular dynamics simulations using an extended air—water interface system. A rectangular cuboid box of the size 24.74 Å  $\times$  24.74 Å  $\times$  100 Å was filled with 512 water molecules and a single  $N_2O_5$  and  $Cl^-$ , creating an air—water interface normal to the z direction. Periodic boundary conditions are applied in all directions. The Lennard-Jones interactions are truncated and shifted at 12 Å. The Ewald summation method is applied to compute long-ranged Coulomb interaction. The equation of motion is integrated by the velocity-Verlet algorithm with a 0.5 fs time step. A Langevin thermostat is applied to fix the temperature at 298 K with a damping constant of 2 ps. All molecular dynamics simulations were performed in LAMMPS  $^{53}$  with the in-house code.

**Free Energy Calculations.** The one-dimensional free energy profiles in Figure 1b are computed from umbrella sampling along z. The density profile of water is decayed to a half of its bulk value at z=0 Å, and positive and negative z correspond to the gas and the solution side, respectively. We prepared 58 independent simulations for each species with harmonic biasing potentials,

$$U(z) = \frac{1}{2}k(z - z_c^i)^2 \tag{9}$$

where  $k = 8 \text{ kcal·mol}^{-1} \text{ Å}^{-2}$  and  $z_{\sigma}^{i}$  the center-of-mass location of species i, are ranging from -12.1 Å to 10.7 Å equally spaced by 0.4 Å. For each simulation, we ran 2.7 ns of production simulation after 0.3 ns of equilibration simulation. Sampled histograms of z are merged together with the weighted histogram analysis method (WHAM),<sup>33</sup> and errors of the free energy are estimated by running 100 bootstrapping trials.<sup>54</sup>

The two-dimensional umbrella sampling used for the free energy surface in Figure 2a was performed by applying two harmonic potentials,

$$U(\xi, z) = \frac{1}{2}k_{\xi}(\xi - \xi_0)^2 + \frac{1}{2}k_z(z - z_0)^2$$
(10)

where  $k_{\xi} = 200 \text{ kcal·mol}^{-1} \text{ Å}^{-2}$ ,  $k_z = 20 \text{ kcal·mol}^{-1} \text{ Å}^{-2}$ ,  $\xi_0$  values are ranging from -0.08 Å to 5.62 Å equally spaced by 0.06 Å, and  $z_0$  values are ranging from -7 Å to 5 Å equally spaced by 0.5 Å. In the vicinity of the transition state, we performed additional simulations with  $k_{\xi} = 400 \text{ kcal·mol}^{-1} \text{ Å}^{-2}$  and  $\xi_0$  values ranging from 0.31 to 0.58 Å equally spaced by

0.03 Å. A total of 2650 independent simulations are performed for 1.8 ns for the production simulation after 0.2 ns of equilibration.

**Bennett–Chandler Calculation.** The transmission coefficients in Figure 2c are computed from an ensemble of trajectories started from the transition state at three fixed z locations: z=-12.3 Å for the bulk, z=0 Å for the interface, and z=5 Å for the gas case. We sampled 300 initial configurations for each case by running a constrained simulation at the transition state. For each configuration, we saved  $\xi$  and  $\Delta s$  values for analysis. Then, we generated 100 different Maxwell–Boltzmann velocities for each configuration and propagated the system for 0.5 ps to let them relax to either the reactant or product basin. Moreover, we repeated the propagation with inverted velocities to improve the convergence of the transmission coefficient using the symmetry

$$\kappa(z,t) = \frac{\langle \nu(0)h_P(\xi(t))\rangle_z^*}{\langle |\nu| \rangle/2} = -\frac{\langle \nu(0)h_P(\xi(t))\rangle_z^*}{\langle |\nu| \rangle/2}$$
(11)

where the indicator functions for the reactant  $(h_R)$  and product  $(h_P)$  states are step-functions which have the kink at initial  $\xi$  values, i.e.,

$$h_{p}(\xi) = \begin{cases} 1 & \text{if } \xi \leq \xi^{*}, \\ 0 & \text{otherwise,} \end{cases}$$
 (12)

where  $\xi^*$  is the transition state value corresponding to the z constraint and  $h_R = 1 - h_P$ . The committor function in Figure 2d,  $P_B(\xi, \Delta s)$ , is defined as the conditional probability of reaching to the product state at t = 0.5 ps given the initial configuration's  $\xi$  and  $\Delta s$  values.

#### ASSOCIATED CONTENT

## **5** Supporting Information

The Supporting Information is available free of charge at https://pubs.acs.org/doi/10.1021/acs.jpclett.4c02289.

Details on the empirical valence band modeling of the reactive system, derivation of the heterogeneous bimolecular rate expression, details on the reaction—diffusion equation modeling, derivation of the analytic uptake coefficients and branching ratio expressions. (PDF)

Transparent Peer Review report available (PDF)

## AUTHOR INFORMATION

#### **Corresponding Author**

David T. Limmer — Department of Chemistry, University of California, Berkeley, California 94720, United States; Kavli Energy NanoScience Institute, Berkeley, California 94720, United States; Materials Sciences Division and Chemical Sciences Division, Lawrence Berkeley National Laboratory, Berkeley, California 94720, United States; orcid.org/0000-0002-2766-0688; Email: dlimmer@berkeley.edu

#### Author

Seokjin Moon — Department of Chemistry, University of California, Berkeley, California 94720, United States;
orcid.org/0000-0003-4939-3266

Complete contact information is available at: https://pubs.acs.org/10.1021/acs.jpclett.4c02289

#### Notes

The authors declare no competing financial interest.

#### ACKNOWLEDGMENTS

The authors thank Gil Nathanson for extensive discussions. D.T.L was supported during the early part of this work by the National Science Foundation through the National Science Foundation Center for Aerosol Impacts on Chemistry of the Environment (NSF-CAICE) under grant number CHE 1801971. D.T.L. acknowledges support from an Alfred P. Sloan Research Fellowship. S.M. was supported by NSF Grant CHE 2102314.

### REFERENCES

- (1) Abbatt, J.; Lee, A.; Thornton, J. Quantifying trace gas uptake to tropospheric aerosol: recent advances and remaining challenges. *Chem. Soc. Rev.* **2012**, *41*, 6555–6581.
- (2) Tie, X.; Brasseur, G.; Emmons, L.; Horowitz, L.; Kinnison, D. Effects of aerosols on tropospheric oxidants: A global model study. *Journal of Geophysical Research: Atmospheres* **2001**, *106*, 22931–22964.
- (3) Limmer, D. T.; Götz, A. W.; Bertram, T. H.; Nathanson, G. M. Molecular Insights into Chemical Reactions at Aqueous Aerosol Interfaces. *Annu. Rev. Phys. Chem.* **2024**, *75*, 111–135.
- (4) Piatkowski, L.; Zhang, Z.; Backus, E. H.; Bakker, H. J.; Bonn, M. Extreme surface propensity of halide ions in water. *Nat. Commun.* **2014**. *5*. 4083.
- (5) Litman, Y.; Chiang, K.-Y.; Seki, T.; Nagata, Y.; Bonn, M. Surface stratification determines the interfacial water structure of simple electrolyte solutions. *Nat. Chem.* **2024**, 644–650.
- (6) Galib, M.; Limmer, D. T. Reactive uptake of N2O5 by atmospheric aerosol is dominated by interfacial processes. *Science* **2021**, *371*, 921–925.
- (7) Cruzeiro, V. W. D.; Galib, M.; Limmer, D. T.; Götz, A. W. Uptake of N2O5 by aqueous aerosol unveiled using chemically accurate many-body potentials. *Nat. Commun.* **2022**, *13*, 1266.
- (8) Davis, J.; Bhave, P.; Foley, K. Parameterization of N 2 O 5 reaction probabilities on the surface of particles containing ammonium, sulfate, and nitrate. *Atmospheric Chemistry and Physics* **2008**, *8*, 5295–5311.
- (9) Brown, S. S.; Stutz, J. Nighttime radical observations and chemistry. *Chem. Soc. Rev.* **2012**, *41*, 6405–6447.
- (10) Dentener, F. J.; Crutzen, P. J. Reaction of N2O5 on tropospheric aerosols: Impact on the global distributions of NO x, O3, and OH. *Journal of Geophysical Research: Atmospheres* **1993**, 98, 7149–7163.
- (11) Alexander, B.; Sherwen, T.; Holmes, C. D.; Fisher, J. A.; Chen, Q.; Evans, M. J.; Kasibhatla, P. Global inorganic nitrate production mechanisms: comparison of a global model with nitrate isotope observations. *Atmospheric Chemistry and Physics* **2020**, *20*, 3859–3877.
- (12) Bertram, T.; Thornton, J. Toward a general parameterization of N 2 O 5 reactivity on aqueous particles: the competing effects of particle liquid water, nitrate and chloride. *Atmospheric Chemistry and Physics* **2009**, *9*, 8351–8363.
- (13) Stewart, D. J.; Griffiths, P.; Cox, R. Reactive uptake coefficients for heterogeneous reaction of N 2 O 5 with submicron aerosols of NaCl and natural sea salt. *Atmospheric Chemistry and Physics* **2004**, *4*, 1381–1388.
- (14) Gaston, C. J.; Thornton, J. A. Reacto-diffusive length of N2O5 in aqueous sulfate-and chloride-containing aerosol particles. *J. Phys. Chem. A* **2016**, *120*, 1039–1045.
- (15) Kercher, J.; Riedel, T.; Thornton, J. Chlorine activation by N 2 O 5: simultaneous, in situ detection of ClNO 2 and N 2 O 5 by chemical ionization mass spectrometry. *Atmospheric Measurement Techniques* **2009**, *2*, 193–204.

- (16) Kelleher, P. J.; Menges, F. S.; DePalma, J. W.; Denton, J. K.; Johnson, M. A.; Weddle, G. H.; Hirshberg, B.; Gerber, R. B. Trapping and structural characterization of the XNO2· NO3–(X= Cl, Br, I) exit channel complexes in the water-mediated X–+ N2O5 reactions with cryogenic vibrational spectroscopy. *J. Phys. Chem. Lett.* **2017**, *8*, 4710–4715.
- (17) Karimova, N. V.; Chen, J.; Gord, J. R.; Staudt, S.; Bertram, T. H.; Nathanson, G. M.; Gerber, R. B. SN2 reactions of N2O5 with ions in water: Microscopic mechanisms, intermediates, and products. *J. Phys. Chem. A* **2020**, *124*, 711–720.
- (18) McCaslin, L. M.; Götz, A. W.; Johnson, M. A.; Gerber, R. B. Effects of Microhydration on the Mechanisms of Hydrolysis and Cl-Substitution in Reactions of N2O5 and Seawater. *ChemPhysChem* **2023**, 24, e202200819.
- (19) Warshel, A. Computer modelling of chemical reactions in enzymes and solutions; Wiley Interscience, 1991.
- (20) Hummer, G. From transition paths to transition states and rate coefficients. *J. Chem. Phys.* **2004**, *120*, 516–523.
- (21) Davidovits, P.; Kolb, C. E.; Williams, L. R.; Jayne, J. T.; Worsnop, D. R. Mass accommodation and chemical reactions at gasliquid interfaces. *Chem. Rev.* **2006**, *106*, 1323–1354.
- (22) Danckwerts, P. Absorption by simultaneous diffusion and chemical reaction into particles of various shapes and into falling drops. *Trans. Faraday Soc.* **1951**, 47, 1014–1023.
- (23) Ballard, A. J.; Dellago, C. Toward the mechanism of ionic dissociation in water. J. Phys. Chem. B 2012, 116, 13490–13497.
- (24) Kattirtzi, J. A.; Limmer, D. T.; Willard, A. P. Microscopic dynamics of charge separation at the aqueous electrochemical interface. *Proc. Natl. Acad. Sci. U. S. A.* **2017**, *114*, 13374–13379.
- (25) Geissler, P. L.; Dellago, C.; Chandler, D.; Hutter, J.; Parrinello, M. Autoionization in liquid water. *Science* **2001**, *291*, 2121–2124.
- (26) Reischl, B.; Köfinger, J.; Dellago, C. The statistics of electric field fluctuations in liquid water. *Mol. Phys.* **2009**, *107*, 495–502.
- (27) Wang, J.; Wolf, R. M.; Caldwell, J. W.; Kollman, P. A.; Case, D. A. Development and testing of a general amber force field. *Journal of computational chemistry* **2004**, *25*, 1157–1174.
- (28) Ou, S.; Hu, Y.; Patel, S.; Wan, H. Spherical monovalent ions at aqueous liquid-vapor interfaces: Interfacial stability and induced interface fluctuations. *J. Phys. Chem. B* **2013**, *117*, 11732–11742.
- (29) Schlegel, H. B.; Sonnenberg, J. L. Empirical valence-bond models for reactive potential energy surfaces using distributed Gaussians. *J. Chem. Theory Comput.* **2006**, *2*, 905–911.
- (30) Mardirossian, N.; Head-Gordon, M.  $\omega$ B97X-V: A 10-parameter, range-separated hybrid, generalized gradient approximation density functional with nonlocal correlation, designed by a survival-of-the-fittest strategy. *Phys. Chem. Chem. Phys.* **2014**, *16*, 9904–9924.
- (31) Wu, Y.; Tepper, H. L.; Voth, G. A. Flexible simple point-charge water model with improved liquid-state properties. *J. Chem. Phys.* **2006**, *124*, 024503.
- (32) Frenkel, D.; Smit, B. Understanding molecular simulation: from algorithms to applications; Elsevier, 2023.
- (33) Kumar, S.; Rosenberg, J. M.; Bouzida, D.; Swendsen, R. H.; Kollman, P. A. Multidimensional free-energy calculations using the weighted histogram analysis method. *J. Comput. Chem.* **1995**, *16*, 1339–1350.
- (34) Loche, P.; Bonthuis, D. J.; Netz, R. R. Molecular dynamics simulations of the evaporation of hydrated ions from aqueous solution. *Communications Chemistry* **2022**, *5*, 55.
- (35) Mentel, T. F.; Sohn, M.; Wahner, A. Nitrate effect in the heterogeneous hydrolysis of dinitrogen pentoxide on aqueous aerosols. *Phys. Chem. Chem. Phys.* **1999**, *1*, 5451–5457.
- (36) Behnke, W.; George, C.; Scheer, V.; Zetzsch, C. Production and decay of ClNO2 from the reaction of gaseous N2O5 with NaCl solution: Bulk and aerosol experiments. *Journal of Geophysical Research: Atmospheres* 1997, 102, 3795–3804.
- (37) Hamlin, T. A.; Swart, M.; Bickelhaupt, F. M. Nucleophilic substitution (SN2): dependence on nucleophile, leaving group,

- central atom, substituents, and solvent. ChemPhysChem 2018, 19, 1315-1330.
- (38) Benjamin, I. Empirical valence bond model of an SN2 reaction in polar and nonpolar solvents. *J. Chem. Phys.* **2008**, *129*, 074508.
- (39) Shaffer, P. R. Ion solvation at air-water interfaces; University of California: Berkeley, 2013.
- (40) Jungwirth, P.; Tobias, D. J. Molecular structure of salt solutions: A new view of the interface with implications for heterogeneous atmospheric chemistry. *J. Phys. Chem. B* **2001**, *105*, 10468–10472.
- (41) Otten, D. E.; Shaffer, P. R.; Geissler, P. L.; Saykally, R. J. Elucidating the mechanism of selective ion adsorption to the liquid water surface. *Proc. Natl. Acad. Sci. U. S. A.* **2012**, *109*, 701–705.
- (42) Schile, A. J.; Limmer, D. T. Rate constants in spatially inhomogeneous systems. *J. Chem. Phys.* **2019**, *150*, 191102.
- (43) Laidler, K. J.; King, M. C. The development of transition-state theory. *J. phys. Chem.* **1983**, *87*, 2657–2664.
- (44) Berne, B. J.; Borkovec, M.; Straub, J. E. Classical and modern methods in reaction rate theory. *J. Phys. Chem.* **1988**, *92*, 3711–3725.
- (45) Chandler, D. Statistical mechanics of isomerization dynamics in liquids and the transition state approximation. *J. Chem. Phys.* **1978**, *68*, 2959–2970.
- (46) Danckwerts, P. V., et al. Gas-liquid reactions; McGraw-Hill: New York, 1970.
- (47) Worsnop, D. R.; Zahniser, M. S.; Kolb, C. E.; Gardner, J. A.; Watson, L. R.; Van Doren, J. M.; Jayne, J. T.; Davidovits, P. The temperature dependence of mass accommodation of sulfur dioxide and hydrogen peroxide on aqueous surfaces. *J. Phys. Chem.* **1989**, 93, 1159–1172.
- (48) Polley, K.; Wilson, K. R.; Limmer, D. T. On the Statistical Mechanics of Mass Accommodation at Liquid-Vapor Interfaces. *J. Phys. Chem. B* **2024**, *128*, 4148–4157.
- (49) Kregel, S. J.; Derrah, T. F.; Moon, S.; Limmer, D. T.; Nathanson, G. M.; Bertram, T. H. Weak Temperature Dependence of the Relative Rates of Chlorination and Hydrolysis of N2O5 in NaCl—Water Solutions. *J. Phys. Chem. A* **2023**, *127*, 1675–1685.
- (50) Pöschl, U.; Rudich, Y.; Ammann, M. Kinetic model framework for aerosol and cloud surface chemistry and gas-particle interactions—Part 1: General equations, parameters, and terminology. *Atmospheric Chemistry and Physics* **2007**, *7*, 5989–6023.
- (51) Hanson, D. R.; Ravishankara, A. Reactive uptake of ClONO2 onto sulfuric acid due to reaction with HCl and H2O. *J. Phys. Chem.* **1994**, *98*, 5728–5735.
- (52) Qiu, L.; Wei, Z.; Nie, H.; Cooks, R. G. Reaction acceleration promoted by partial solvation at the gas/solution interface. *ChemPlusChem.* **2021**, *86*, 1362–1365.
- (53) Thompson, A. P.; Aktulga, H. M.; Berger, R.; Bolintineanu, D. S.; Brown, W. M.; Crozier, P. S.; in't Veld, P. J.; Kohlmeyer, A.; Moore, S. G.; Nguyen, T. D.; et al. LAMMPS-a flexible simulation tool for particle-based materials modeling at the atomic, meso, and continuum scales. *Comput. Phys. Commun.* **2022**, 271, 108171.
- (54) Grossfield, A. WHAM: an implementation of the weighted histogram analysis method; University of Rochester, USA, 2011.